Biophysical Chemistry 184 (2013) 108–115

Contents lists available at ScienceDirect

Biophysical Chemistry

journal homepage: http://www.elsevier.com/locate/biophyschem

Surface induced collapse of $A\beta_{1\text{-}42}$ with the F19A replacement following adsorption on a single walled carbon nanotube

Asis K. Jana, Neelanjana Sengupta *

Physical Chemistry Division, CSIR-National Chemical Laboratory, Mr. Homi Bhaba Road, Pune 411008, India

HIGHLIGHTS

- Simultaneous reduction of hydrophobic and aromatic character in central hydrophobic core of Aβ monomer investigated.
- Propensities for intrinsic collapse and adsorption on SWCNT surface is reduced.
- Favorability of the 'anomalous' surface induced collapse verified with free energy calculations.
- Lateral movement on surface due to weakened adsorption leads to interactions with C-terminal domain.
- Collapse of the adsorbed peptide leads to further loss of surface hydration.

GRAPHICAL ABSTRACT

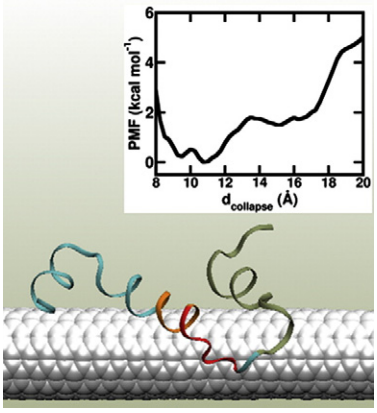

ARTICLE INFO

Article history:
Received 21 August 2013
Received in revised form 25 September 2013
Accepted 28 September 2013
Available online 30 October 2013

Keywords:
Amyloid beta peptide
Carbon nanotube
Molecular dynamics simulation
Adsorption
Surface induced collapse
Lateral mobility

ABSTRACT

Spontaneous adsorption of the Aβ peptide on the surface of a single-walled carbon nanotube, resulting in the prevention of its intrinsic propensity to form collapsed states, could be a plausible means to hinder the peptide's initial nucleation and self-assembly. We report here the effects of sharply reducing both aromatic and hydrophobic character within the peptide's central hydrophobic core on its free and surface behavior. In such an altered peptide, complete surface adsorption is found to induce, rather than prevent, the adsorbed peptide's collapse. The weakened surface interactions of the central hydrophobic core allow its greater translational mobility on the surface, thereby facilitating interactions that lead to compaction. Both the adsorption and the subsequent collapse are accompanied by a loss of surface hydration in the modified peptide. We further find that such a two-step dewetting leads to hydration levels comparable to that obtained after compaction of the free peptide. These insights may be leveraged for designing molecular surfaces for disrupting intrinsic Aβ behavior.

1. Introduction

The advent of novel nanomaterials has opened up a variety prospects in biotechnology and medicine [1,2]. Particularly, the possibility of harnessing the unique properties of carbon-based nanomaterials in order to render them useful in biomedical applications and therapeutics is under intense investigation, while keeping in mind several issues pertaining to cellular toxicity and potential side effects [3,4]. These ideas have fueled studies aimed at understanding the influence exerted by such nanomaterials on cellular machinery, and have necessitated research at the 'single-molecule' level of their interactions with biomolecules such as carbohydrates, lipids, peptides and proteins, and nucleic acids [5–10]. Detailed knowledge of the nature of these interactions,

* Corresponding author. Tel.: +91 20 2590 2087; fax: +91 20 2590 2636.
E-mail address: n.sengupta@ncl.res.in (N. Sengupta).

0301-4622/$ – see front matter © 2013 Elsevier B.V. All rights reserved.
http://dx.doi.org/10.1016/j.bpc.2013.09.008

their dependence on nanomaterial size, shape, curvature, effective hydrophobicity, surface exposure and solubility, and their subsequent optimization may plausibly pave the way for effective applications of carbon based nanomaterials in biology.

Recently, there have been efforts to understand if carbon based nanomaterials such as fullerene [11], graphene oxide [12] and carbon nanotubes [13–15] can be used to alter the properties of Amyloid beta (Aβ), an intrinsically unstructured peptide strongly implicated in Alzheimer's disease (AD), a neurodegenerative proteopathy. According to the amyloid hypothesis, the self-assembly of the Aβ sequence, itself created from enzymatic cleavage of the much larger, membrane embedded Amyloid precursor protein (APP) into insoluble fibrillar plaques, and their deposition into neuronal synapses of the brain, triggers the onset of AD [16]. Recent research, however, strongly implicates soluble oligomers of Aβ as the most neurotoxic species [17], and recent efforts have sought to characterize the structure and size distribution of such entities and how they are associated with solvent and thermodynamic conditions [18–21]. The discovery of means to hinder self-assembly pathways of the Aβ monomer or to destabilize its fibrillar aggregates, and detailed understanding of the underlying physico-chemical mechanisms could pave the way for novel AD therapeutics.

A large subset of the Aβ peptide's biophysical properties appears to be strongly correlated to the physico-chemical behavior of key domains, particularly the central hydrophobic core ($L_{17}VFFA_{21}$) [22,23], the turn region [24–26], and parts of the C-terminal domains ($G_{29}AIIGLMVGGVVIA_{42}$) [23,27]. These domains play important roles in the peptide's self-assembly mechanisms, and some proposed AD therapeutic strategies target one or more of these regions [28,29]. Single-point mutations in these domains have been noted to alter the peptide's structural and self-assembly properties [30–32]. Aβ attains compact states in fully aqueous environment, and the collapse is considered an early step in the peptide's nucleation and consequent self-assembly [27,33,34]. Using atomistic molecular dynamics (MD) simulations, we recently showed that the 42-residue Aβ peptide adsorbs spontaneously on the surface of a single-walled carbon nanotube (SWCNT) of small diameter [14]. Consequently, key interactions between the central hydrophobic core (HP1) and the C-terminal domains were severely hindered, which resulted in preventing the peptide's collapse and populating the 'open' states. We further highlighted the competition between the adsorption and collapse processes, showing that a dewetting transition initiated by HP1, and subsequent π−π stacking which consolidated its interactions with the nanotube, are essential for the peptide's complete adsorption on the nanotube surface [15].

In this paper, we report our observations of the behavior of the Aβ peptide, both on the surface of a carbon nanotube, as well as an isolated monomer, by a strong and simultaneous reduction in both the overall hydrophobic and aromatic character of HP1. This has been achieved by replacing Phe19 with Ala, whose hydrophobicity index of 0.31 based on water/octanol partitioning is significantly lower than that of Phe (1.80) [35]. While the propensity for either the (free) peptide's collapse or its SWCNT adsorption did not disappear, the weakening of key interactions severely diminished the probability of either phenomenon. Interestingly, in sharp contrast with our previous observations, the nanotube surface induced, rather than prevented, the compaction of the peptide in the event of complete adsorption of the F19A altered peptide. Adaptive biasing force (ABF) based free energy calculations performed on the pre-adsorbed F19A peptide corroborate the thermodynamic favorability of the peptide collapse. The weaker surface interactions allow a greater degree of lateral movement of HP1 on the nanotube surface, effectively facilitating interaction with the C-terminal domain and inducing marked compaction. The dewetting resulting from the post-adsorption collapse of F19A is comparable to that resulting from spontaneous collapse on the unmutated peptide. Our studies directly demonstrate the critical dependence of observed surface and biophysical characteristics of the Aβ sequence on the overall chemical nature of its key domains. The insights gained may have important ramifications in the design of molecular surfaces for disrupting intrinsic Aβ behavior.

2. Computational methods

2.1. System setup and MD simulations

The initial peptide–SWCNT setup is depicted in Fig. 1. The coordinates for $Aβ_{1-42}$, obtained with solution NMR studies of full-length Aβ in the 'lipid-mimicking' environment of a 3:7 mixture of water and hexafluoro-2-propanol, were taken from the PDB database (PDB ID: 1Z0Q) [36], while those for the (6, 6) SWCNT of 8.2 Å diameter were obtained with the VMD package [37]. We mention here that the evolution in water of the peptide structure used here, and other related structures [38,39] is considered analogous to the pathway of the freshly cleaved peptide released in aqueous cytoplasm [36,40,41]. Furthermore, these structures are extensively used in computational studies to understand Aβ monomeric behavior in water and at interfacial environments [41–44]. The initial peptide-nanotube complex was set up in the 'NT2A' configuration, which is identical to the 'NT2' configuration reported previously, except for the substitution of Phe19 with Ala. We have earlier shown that the adsorption mechanism is independent of the initial peptide-nanotube orientation [14]. NT2 had the least initial peptide-nanotube contact area of all the initial configurations studied earlier, and hence the adsorption mechanism was most clearly discernible in this system. In the NT2/NT2A configurations, the HP1 and N-terminal domains were farthest from the nanotube surface, and the C-terminal domain was initially set parallel to the nanotube axis, with its center of mass 8.5 Å away from the surface, resulting in low initial peptide-nanotube contact area. The SWCNT atoms were held fixed with harmonic forces and the nanotube axis oriented parallel to the x-axis. Periodic boundary conditions were used to create infinitely long SWCNTs. NH_3^+ and COO^- groups were attached, respectively, to the N- and C-terminii of Aβ. Three Na^+ counterions were added for charge neutrality, and the TIP3P [45] water model was used to solvate the resulting complex with about 9500 water molecules. The free peptide containing the Ala replacement was similarly setup, and about 9400 water molecules were used. The peptide with the Ala mutation has been referred to as 'F19A'. Six independent simulation runs, each of 100 ns duration were obtained for the NT2A systems, and three independent runs were generated for the F19A systems. Adaptive biasing force based free energy calculations were further performed to probe the NT2A systems (see below). Corresponding data for the unmutated systems have been reported earlier [14].

MD simulations were performed with the CHARMM22 all-atom force field with the CMAP corrections [46,47] using the NAMD simulation package [48]. Bonds with hydrogen atoms were constrained using the SHAKE algorithm [49]. The conjugate gradient method was first used to initially energy minimize on each system for 10000 steps, following which simulations were carried out in the isothermal-isobaric ensemble with a temperature of 310 K and a pressure of 1 atm, using a timestep of 2 fs. Langevin dynamics with a collision frequency of 1 ps^{-1} was used to maintain constant temperature, and constant pressure was maintained via the Langevin piston Nosé–Hoover algorithm, using Langevin piston period and decay of 200 fs [50,51]. Three-dimensional orthorhombic periodic boundary conditions were used and electrostatic interactions were calculated with particle-mesh Ewald [52]. The non-bonded interaction cutoff was 12 Å, with smoothing started at 10.5 Å.

2.2. Adaptive biasing force calculations

To characterize the energetic favorability of collapse of the F19A peptide adsorbed on the SWCNT surface, the potential of mean force (PMF) was calculated with the adaptive biasing force (ABF) method as implemented in the NAMD package which was used [53,54]. As earlier, the center of mass distance between the segments $L_{17}VFFAEDVGS_{26}$ and

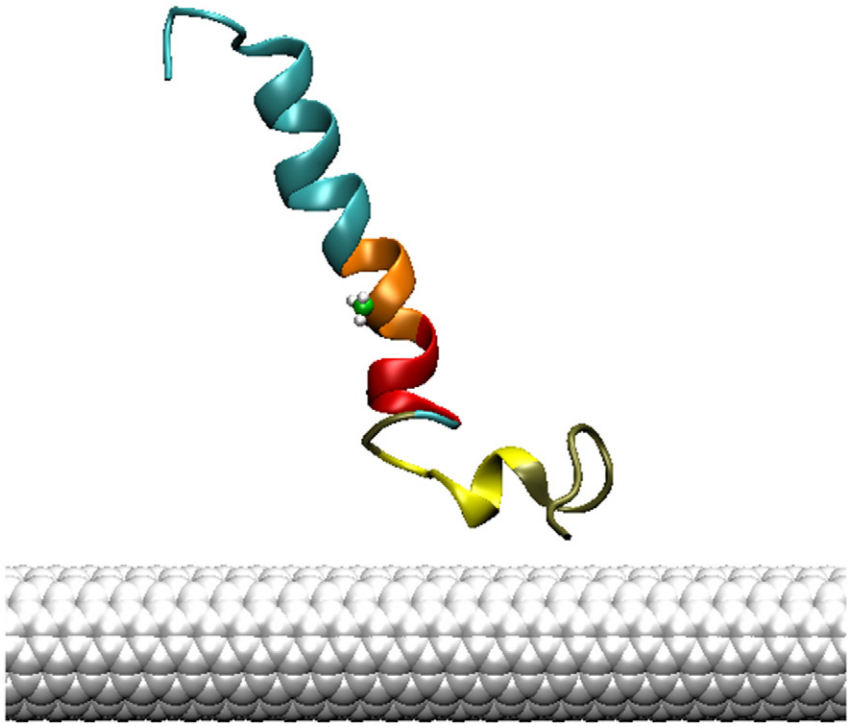

Fig. 1. Initial setup of the A$\beta_{1\text{-}42}$-SWCNT complex with F19A mutation. The N-terminal region (D_1AEFRHDSGYEVHHQK$_{16}$) is depicted in cyan. The segment L_{17}VAFAEDVGS$_{26}$ is depicted in red-orange color, with the central hydrophobic core (HP1) highlighted in orange, and the Ala sidechain at position 19 highlighted in CPK representation. The K_{28}GAIIGLMVGGVVIA$_{42}$ domain is depicted in yellow-tan color, with the HP2 domain (A_{30}IIGLM$_{35}$) shown in yellow.

K_{28}GAIIGLMVGGVVIA$_{42}$ (or '$d_{collapse}$') was chosen as the reaction coordinate to describe peptide compactification [14]. Initial coordinates were taken from a snapshot obtained just after the peptide had reached saturated $A_{contact}$ value. The ABF method is a thermodynamic integration formalism wherein the average force acting along a particular reaction coordinate (say ζ) is used to estimate the bias required for overcoming local barriers in the free energy iso-surface. With a single dimensional surface, the gradient of the free energy A is calculated from the average force exerted on ζ, i.e.,

$$\frac{dA(\zeta)}{d\zeta} = -\left\langle F_\zeta \right\rangle_\zeta$$

F_ζ accumulated in small bins over the range of interest is used to estimate the biasing force required to overcome local free energy barriers.

In this study, $d_{collapse}$ ranged from 8 to 21 Å and was divided into 52 windows, each 0.25 Å wide. Unbiased sampling was obtained for 500 steps before estimation and application of the bias in order to avoid non-equilibrium effects. The ABF simulations were carried out for more than 200 ns, and the free energy profile reported converged over a period of 50 ns. The maximum extent of error for the free energy calculation was estimated using the methodology proposed by Rodriguez-Gomez [55,56].

3. Results

3.1. Effect of F19A mutation on free peptide collapse

The Aβ monomer displays a strong propensity to form collapsed states in water that can potentially nucleate and initiate heterogeneous self-assembly pathways. As in our previous studies, we monitor the compaction of the peptide via the value of '$d_{collapse}$', the center of mass distance between the N-terminal (L_{17}VXFAEDVGS$_{26}$) and C-terminal (K_{28}GAIIGLMVGGVVIA$_{42}$) domains, with the 'X' at position 19 representing the modification. We have demonstrated earlier that $d_{collapse}$ is temporally well correlated with E_1, the interaction strength between HP1 and HP2, and that E_1 provides the major component of E_2, the interaction between HP1 and the full C-terminal domain. We mention here that interaction strength between two groups includes the sum of the non-bonded (electrostatic and van der Waals) interaction energies. Collapse was taken to have occurred if $d_{collapse}$ decreased by 30% or more from the original value of 16.7 Å. To understand the effect of the F19 mutation on this essential self-assembly step, we first depict the normalized probabilities of $d_{collapse}$ values obtained during the last 10 ns of the simulated F19A trajectories in Fig. 2A. The plot describes two distinct groups of 'collapsing' and 'non-collapsing' structures. The mean $d_{collapse}$ of 9.6 ($\pm$0.3) Å of the former group is comparable to that of the mean value obtained for the pure, unmutated peptide, while the mean value of 17.0 ($\pm$1.2) Å for the latter group represents structures that remain significantly more 'open' at the end of the simulations. In Fig. 2B, we have depicted evolution of the peptide's radius of gyration (R_g) with that of $d_{collapse}$, E_1 and E_2 for representative 'collapsing' and 'non-collapsing' trajectories. Further, as in the unmutated systems, the strong correlation of R_g and $d_{collapse}$ with one but not all the three principle moments of inertia depicts that the peptide's compaction arises mainly due to the strand–strand collapse (see Fig. S1 in Supplementary Material).

In Table 1, we have compared the mean values of R_g, $d_{collapse}$, E_1 and E_2, as well as the probability of peptide collapse obtained from the F19A simulations and the previously reported simulations of the unmutated peptide. We had reported earlier that while the F19I appeared to have no significant effect on the collapse probability of the peptide in water, the F19Y mutation diminished this probability by 33%. In the current study, only one out of the three simulated F19A trajectories is found to achieve collapse. We note here that the interactions E_1 and E_2 for the collapsing F19A trajectory are marginally weaker than the

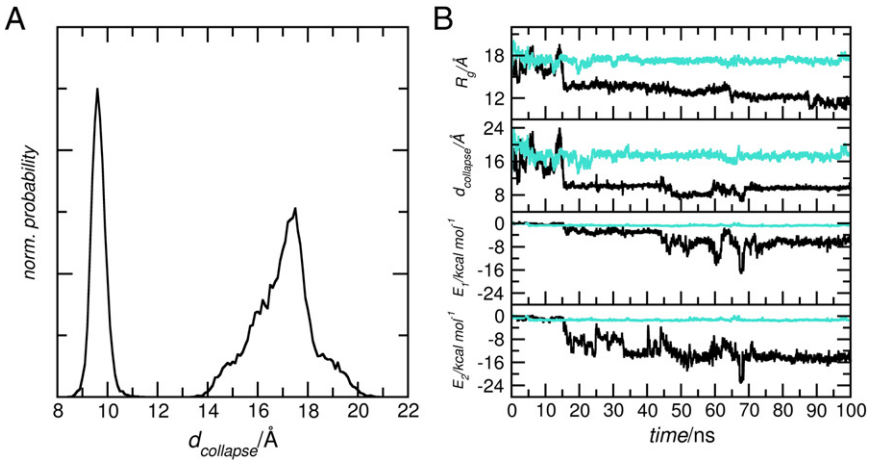

Fig. 2. A) Normalized distributions of $d_{collapse}$ (in Å) value obtained from the last 10 ns of the simulated free F19A peptide. B) Evolution of peptide radius of gyration, R_g (in Å), $d_{collapse}$ (in Å), and the interactions E_1 and E_2 (in kcal mol^{-1}) over the simulation time, for a sample collapsing (in black) and non-collapsing (in cyan) free F19A peptide.

corresponding values obtained in the unmutated peptide. This data shows that the effective hydrophobicity of the HP1 domain is requisite for the efficient collapse kinetics of the nascent Aβ monomer in aqueous environment.

3.2. Propensity for SWCNT adsorption

We next investigate the combined effect of decreased aromatic character and reduced effective hydrophobicity in HP1 on the peptide's adsorption propensity on the SWCNT. The peptide-nanotube contact area, or $A_{contact}$, calculated as described in the previous studies was used to monitor adsorption. As in our previous studies, the peptide is considered to have fully adsorbed on the SWCNT if a minimum $A_{contact}$ of 800.0 Å^2 is achieved. From our earlier extensive simulations, we found that the unmutated peptide compulsorily adsorbs on the surface of the SWCNT placed in its vicinity within tens of nanoseconds irrespective of the initial peptide-nanotube orientation. In comparison, replacement of Phe19 with either Ile or Tyr caused a marked decrease in the overall adsorption propensity. However, in each case, an adsorption event resulted in prevention of the peptide's collapse. We further noted that the adsorption of the N-terminal domain, which was essential for attainment of the saturated $A_{contact}$ value, was dependent on the prior interaction of HP1 with the SWCNT. In Table 2, we report the mean $A_{contact}$ and $d_{collapse}$ values obtained over the last 10 ns of the NT2A simulations, along with the mean interaction strength of the nanotube with the full peptide, the HP1 domain, and the C-terminal region. For comparison, we have also reported corresponding mean values obtained from the previous simulations of unmutated peptide–SWCNT complex. As indicated by the difference in $A_{contact}$ value, the F19A mutation results in a 26% decrease in the mean adsorption propensity. Further, the mean $d_{collapse}$ value is 27% lower compared to the unmutated peptide–SWCNT complex within the simulated timescales.

Out of our six simulations of the NT2A complex, the peptide was found to adsorb on the SWCNT surface in only two, indicating a lower probability of complete adsorption compared to the systems studied earlier. In Fig. 3, we depict normalized distributions of the value of $A_{contact}$ obtained by combining data from the last 10 ns of all the simulated trajectories; for comparison, the corresponding distribution from NT2 has also been shown. The data indicates the presence of three distinct groups, which we denote here as groups 1, 2 and 3, with mean $A_{contact}$ values of 500.5 (±28.8) Å^2, 660.0 (±29.1) Å^2 and 889 (±60.3) Å^2. In the same figure, we also show temporal evolution of the contact area of the key domains (N-terminal domain; HP1; HP2 and C-terminal domain) with the SWCNT over sample trajectories corresponding to each of the three groups.

In Table S1 in Supplementary Material, we have reported the mean $A_{contact}$ and $d_{collapse}$ of the different domains for the three groups obtained over the final 10 ns of the simulations along with the mean contact area of the key domains. For comparison, earlier data corresponding to the NT2 system has also been presented. As earlier, we find that stable adsorption of the HP1 domain is a prior requisite for complete N-terminal adsorption of the peptide; the latter provides a large fraction of the $A_{contact}$ corresponding to complete adsorption. However, we note that in the case of group 2, the HP1-SWCNT interaction yields only partial N-terminal adsorption on the nanotube. Interestingly, unlike the previous systems studied, we find that the complete adsorption of the F19A system on the SWCNT gives rise to a low value of $d_{collapse}$. While this value is marginally higher than that corresponding to collapse of the free peptide (native or mutated), it is 41% less than the mean $d_{collapse}$ attained at the end of the NT2 simulation (we underscore here that in the earlier systems studies, complete adsorption was shown to erase the natural collapse propensity). This unexpected behavior has been examined in greater details in subsequent sections.

3.3. Post-adsorption peptide collapse in NT2A

We introspect the phenomenon of post-adsorption collapse observed in the NT2A systems. In Fig. 4, we present plots of $A_{contact}$ and $d_{collapse}$ as a

Table 1
Comparison of mean values of R_g (in Å), $d_{collapse}$ (in Å), E_1 (in kcal mol^{-1}) and E_2 (in kcal mol^{-1}) over the last 10 ns of free F19A and unmutated simulations. Standard deviations are provided in braces.

System	R_g	$d_{collapse}$	E_1	E_2
F19	12.1	8.3	−10.1	−17.4
	(0.5)	(0.9)	(−2.8)	(−4.4)
F19A	15.0	14.5	−2.9	−6.1
	(2.7)	(3.6)	(2.7)	(6.2)

Table 2
Comparison of the mean $A_{contact}$ (in Å^2), $d_{collapse}$ (in Å), full peptide-nanotube interaction (E_{3a}), HP1-nanotube interaction (E_{3b}), C-terminal domain-nanotube interaction (E_{3c}) obtained over last 10 ns of all the simulated NT2A and NT2 trajectories. Energies are in kcal mol^{-1}. Standard deviations are provided in braces.

System	$A_{contact}$	$d_{collapse}$	E_{3a}	E_{3b}	E_{3c}
NT2	935.6	19.05	−130.0	−17.0	−37.8
	(52.7)	(5.0)	(8.5)	(2.6)	(7.4)
NT2A	691.6	13.9	−96.0	−8.0	−39.5
	(176.3)	(2.6)	(23.4)	(5.6)	(3.8)

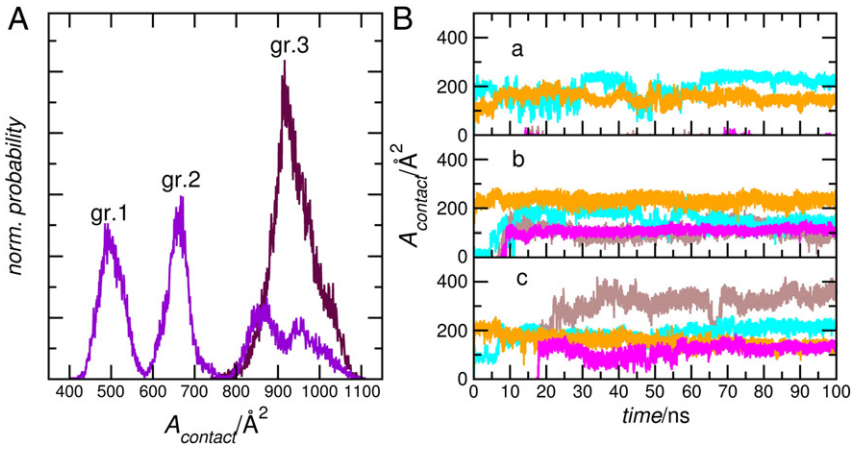

Fig. 3. A) Normalized distribution of $A_{contact}$ values obtained from the last 10 ns of the simulated NT2A systems (in violet) compared to the NT2 systems (in maroon), and B) evolution of nanotube contact area of key domains for representative trajectories belonging to a) gr. 1, b) gr. 2, and c) gr. 3. See text for details. Contact area with HP1 is in magenta; with residues 1 to 16 in light brown; with residues 30 to 35 in orange; and with residues 36 to 41 in cyan.

function of simulation time for the trajectories that are found to completely adsorb within the simulated timescale. The saturation in $A_{contact}$ is followed by a lag period (of ~30–40 ns duration), after which the peptide is found to dramatically compactify by attaining a $d_{collapse}$ of 11.2 Å. However, the lowered adsorption probability yielded just two completely adsorbed trajectories, and therefore it remained to be unequivocally determined whether the collapse observed upon F19A adsorption is indeed surface induced. To this end, we present the PMF profile calculated via ABF as described earlier in Fig. 5, with the complex achieved just after attaining saturated $A_{contact}$ ($d_{collapse}$ of 17.0 Å) as the starting conformation. The free energy data indicates a downhill transition to the 'closed' states for the peptide. The highest probability is found in the vicinity of a $d_{collapse}$ value of 10.75 Å, which is very close to the mean $d_{collapse}$ value of the fully adsorbed peptide obtained through unbiased sampling of the NT2A systems (see Supplementary Material). In contrast, the 'open' states (corresponding to $d_{collapse}$ values greater than the original value of 16.7 Å) of the adsorbed peptide correspond to high free energy values and thus the probability of sampling those states is low. It is easily seen that for the complex studied, there is an energetically favorable downhill transition to the 'closed' states from the starting $d_{collapse}$ value. This is in contrast to unmutated NT2 system, in which the free energy profile over $d_{collapse}$ describes a downhill transition to the 'open' states [14]. We note, however, that the surface induced collapse is marginally weaker compared to the free peptide collapse (see Table S2 for a comparison of E_2 values).

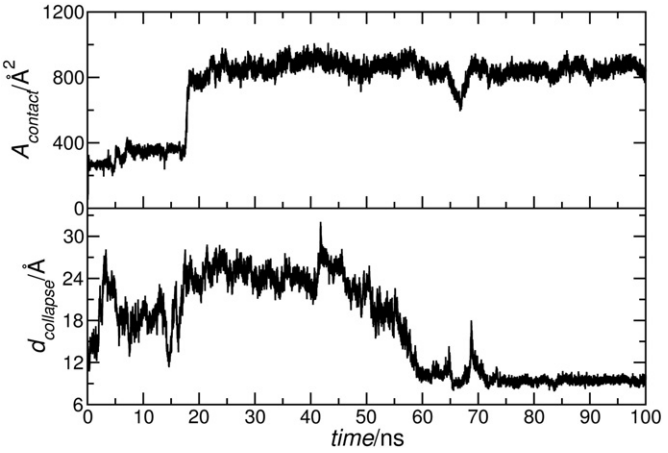

Fig. 4. Evolution of $A_{contact}$ (in upper panel) and $d_{collapse}$ (in lower panel) over simulation time for a sample, fully adsorbing NT2A trajectory.

3.4. Enhanced movement on nanotube surface arising from weakened tethering of HP1 in NT2A

For mechanistic insights into the role played by the SWCNT in facilitating collapse of the fully adsorbed peptide in NT2A, we begin by re-examining the mean interaction strengths of different domains with the nanotube surface. In the case of the fully adsorbed NT2A, we note that a large part of the difference in overall peptide-nanotube interaction (in comparison with NT2) is accounted for by the weakened interaction of HP1 with the nanotube. In Fig. 6, we have compared distributions of the HP1-nanotube contact area for 20 ns after adsorption, between the NT2A (fully adsorbing) and the NT2 systems. The mean HP1-nanotube contact area values for the two systems are 147.4 (±23.0) and 179.5 (±18.5) Å^2, respectively. In the same figure, we also depict evolution of the radial distance of the center of mass of HP1 from the nanotube for these systems. The sharp drop in the in the radial distances is indicative of HP1 localization on the nanotube surface following complete adsorption. This data, along with the lower mean contact area and the distinctly broader HP1-nanotube contact area distribution, indicate that the peptide in NT2A is less stably adsorbed and weakly tethered to the nanotube surface. We do not notice any meaningful differences in interaction of the nanotube with the C-terminal domain.

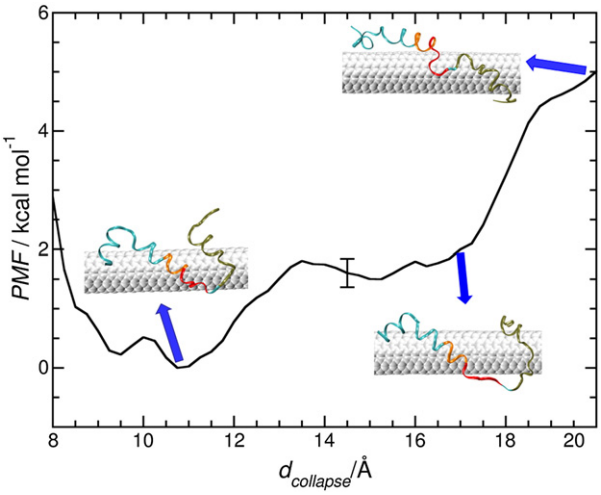

Fig. 5. The free energy profile along $d_{collapse}$ for the peptide in a completely adsorbed NT2A trajectory obtained with ABF calculations. Snapshots of the adsorbed peptide–SWCNT complex corresponding $d_{collapse}$ values of 11.0 Å, 17.0 Å and 20.0 Å along the profile are shown.

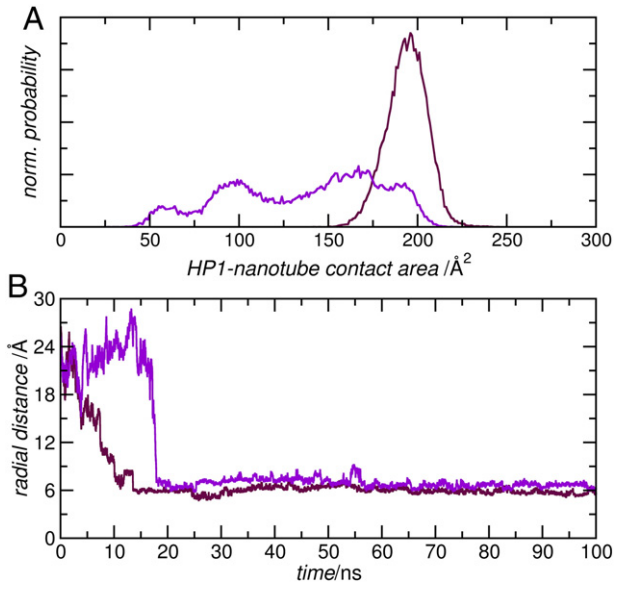

Fig. 6. A) Comparison of the HP1-nanotube contact area distribution, calculated for 20 ns after adsorption, between the fully adsorbing NT2A (in violet) and the unmutated NT2 (in maroon) systems, and B) comparison of the evolution of the radial distance of the HP1 domain's center of mass from the nanotube surface, for a sample fully adsorbing NT2A (in violet) trajectory and NT2 trajectory (in maroon).

To directly compare the extent of domain mobility on the nanotube surface in the two cases, we depict in Fig. 7 the distances (Δd) moved by the HP1 domain center of mass between consecutive frames (i.e. every picosecond), as a function of simulation time for representative NT2A and NT2 trajectories. Although the adsorption event in both cases is marked by diminished movement of this domain, its weakened tethering allows it to have greater translational mobility on the surface in the NT2A complex compared to NT2. However, the C-terminal tethering combined with the 'hairpin'-like conformation of the peptide restricts its mobility parallel to the nanotube axis (i.e. along the x-axis). Thus, the Δd is well correlated with the transverse movement on the nanotube surface (i.e. with Δd_{yz}), as shown in the same figure. Corresponding data for the C-terminal domains show no clear differences in the extent of movements in NT2 and NT2A (see Fig. S2). The 'restricted random walk' of the HP1 domain in the adsorbed NT2A system dramatically increases its likelihood of coming within approach distance of HP2 and the C-terminal domains. Thus, after a post-adsorption lag phase (corresponding to an 'open' state with higher $d_{collapse}$ value), strong interactions between HP1 and the C-terminal two domains result in compaction of the peptide.

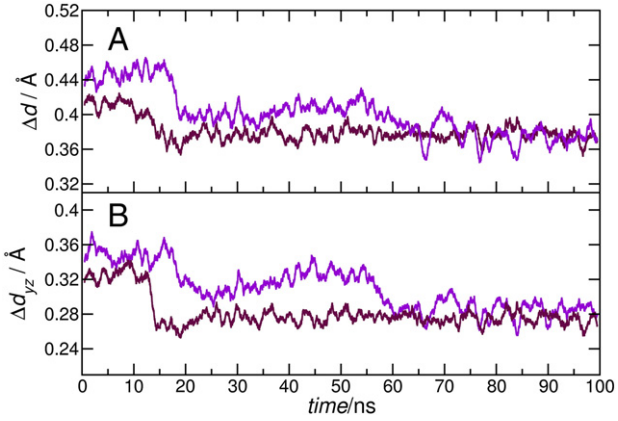

Fig. 7. A) The distances (Δd) moved by the HP1 center of mass between consecutive steps as function of simulation time, for representative fully adsorbing NT2A (in violet) and NT2 (in maroon) trajectories, and B) evolution of the component Δd_{yz} over the simulation time.

3.5. Dewetting effects in free and surface induced collapse

We have earlier shown that peptide adsorption on the surface is accompanied by a distinct dewetting transition at the HP1 domain in NT2, NT2I and NT2Y systems [15]. Here, we examine the dewetting due to complete peptide adsorption, and that induced by the subsequent collapse in NT2A. In Fig. 8, we present comparisons of the radial distribution functions (RDFs) of water oxygen around the terminal carbon atoms of HP1 domains F19A (collapsing) and NT2A (adsorbing) trajectories, before and after collapse for the former, and before and after adsorption and after collapse for the latter. Corresponding data for the F19 and NT2 systems is shown in Fig. S3. We first note that in the unmutated systems, the drop in the height of the first solvation peak located at 3.7 Å is nearly due to collapse (of the free system) and due to SWCNT adsorption, and further, this is comparable due to the dewetting from collapse of the free F19A peptide. With the Ala mutation, however, full peptide adsorption does not result in complete dewetting as seen from the larger first solvation peak of the terminal carbons of HP1 post-adsorption. Interestingly, the collapse transition following the adsorption brings a distinct lowering in the first solvation peak and eventually makes it comparable to that obtained from the free collapse. Thus, the event of complete peptide adsorption in NT2A, the reduced degree of peptide solvation is achieved via a 'two-step' dewetting involving the peptide's collapse. This is also evidenced by comparing the hydration number within 3.0 Å of the heavy atoms of HP1 before and after adsorption and collapse in the free peptide and the peptide–SWCNT complex, reported in Table 3. The hydration numbers in F19A are slightly lower despite the lower hydrophobicity of Ala compared to Phe; this is due to the lower van der Waals volume of Ala [57]. In Fig. S4, we have compared evolutions of the number of surface waters around HP1 for a sample NT2A (adsorbing) trajectory. We note here that recent studies have demonstrated the importance of surface hydration in the self-assembly thermodynamics of Aβ. The net entropic gain due to expulsion of surface waters during peptide compaction and during monomeric association and the consequential energetic favorability have been elaborated [58]. It is plausible therefore that the second dewetting transition in NT2A contributes to the thermodynamic favorability of collapse in the adsorbed peptide. We note here that compared to the unmutated peptide, the peptide in (absorbing) NT2A complex is relatively more stabilized due to the post-adsorption collapse (see Table S3). Further detailed studies will be required to directly validate the role played surface waters in the observed phenomena.

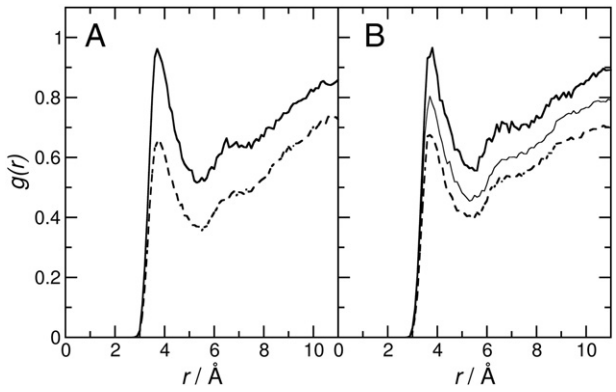

Fig. 8. Radial distribution functions (RDFs) of water oxygens around the terminal carbons of the HP1 domain obtained from A) collapsing F19A free peptide simulation, B) fully adsorbing NT2A simulation. The RDFs are over the initial 10 ns in both (solid thick line), 10 ns after adsorption in NT2A (solid thin line), and 10 ns after collapse (broken line).

Table 3
The initial hydration (W_i) number of HP1 compared to that after collapse (W_c), and after adsorption (W_a), for the peptide in the NT2A (fully adsorbing) and NT2 systems, and for the free peptide in the F19A (collapsing) and F19 systems. Data is averaged over 10 ns. Standard deviations are provided in braces.

System	W_i	W_a	W_c
NT2	21.7	15.2	–
	(4.1)	(3.8)	
NT2A	19.1	16.0	12.1
	(3.5)	(3.4)	(3.0)
F19A	18.5	–	12.6
	(3.5)		(3.1)
F19	21.9	–	15.2
	(3.8)		(3.3)

4. Discussion and conclusion

In this paper, we have reported the behavior of the full-length Aβ, modified at its central hydrophobic core (HP1) by the F19A replacement, on the surface of a single-walled carbon nanotube of small diameter. In the unmutated peptide, strong interactions of this domain with the nanotube had earlier been reported to bring about rapid and spontaneous adsorption on the nanotube surface, with the HP1 playing a key role in the formation of the stable peptide-nanotube complex. The simultaneous reduction in both hydrophobic and aromatic character within this domain dramatically reduces the propensity for complete peptide adsorption and the propensity for free collapse. Compared to the natural sequence where there is 100% adsorption, only two out of six F19A altered peptide–SWCNT complexes are found to fully adsorb within the simulated timescales. The incomplete interaction of the HP1 domain is found to hinder the complete N-terminal interaction. The mutual exclusivity of collapse and complete adsorption observed earlier is found to be absent in the case of the F19A system. On the contrary, complete peptide adsorption is necessarily followed by peptide compaction on the surface; this is corroborated with free energy calculations. Weakened tethering of HP1 results in its 'restricted random walk' on the surface, thereby facilitating its interaction with the hydrophobic C-terminal domains.

Our study underscores the critical nature of the Aβ sequence in bringing about its recognizable biophysical behavior. Even minor alterations to the natural sequence could result in marked differences in intrinsic thermodynamic and kinetic properties of the peptide. This is particularly the case for the HP1 domain, whose physico-chemical properties arising out of its sequential integrity are key to several structural transitions of the peptide after its cleavage from the precursor and release into the aqueous cytoplasm. Our results thus ratify the appropriateness of recent therapeutic strategies that seek to alter intrinsic self-assembly behavior and stability of Aβ by targeting the HP1 domain.

Before concluding, we note the recent body of research highlighting interfacial behavior of proteins, including those of amyloidogenic proteins such as Aβ [43,44,59,60]. It has been shown that protein adsorption on surfaces may lead to altered activity and stability, and may induce self-assembly by reducing the dimensions available for translational mobility from three to two. In the light of these observations, it is important to clearly correlate interfacial behavior with the nature of the interface, the specificity of its interactions with particular protein domains, and possible solvent effects. Our results describing how small perturbations to the Aβ sequence are capable of dramatically altering its interfacial behavior on a hydrophobic surface, should have important bearings upon studies of nucleation and self-assembly at interfaces.

Acknowledgment

The authors are grateful for the financial assistance provided through the Multi-Scale Simulation and Modeling project (MSM), CSIR. CSIR-NCL, Pune, is acknowledged for funds and facilities provided through the Centre of Excellence in Scientific Computing. Financial assistance from the Center of Excellence in Polymers (CoEP-SPIRIT), established from funding received from the Department of Chemicals and Petrochemicals is acknowledged. A.K.J. thanks the University Grants Commission for his current Junior Research Fellowship.

Appendix A. Supplementary data

Supplementary data to this article can be found online at http://dx.doi.org/10.1016/j.bpc.2013.09.008. This material provides evolution of principle moments of inertia of collapsing and non-collapsing F19A; movement of C-terminal domain for fully adsorbing peptide in NT2A and NT2 trajectories; water-terminal carbon radial distribution function for HP1; solvation number around HP1; mean contact areas of key domains for NT2A and NT2; HP1-C-terminal domain interactions for F19A and NT2A systems; total internal energy of peptide in NT2A and NT2.

References

[1] V. Wagner, A. Dullaart, A.K. Bock, A. Zweck, Nat. Biotechnol. 24 (2006) 1211–1217.
[2] W.T. Al-Jamal, K. Kostarelos, Acc. Chem. Res. 44 (2011) 1094–1104.
[3] Y. Wenrong, P. Thoradarson, J.J. Gooding, S.P. Ringer, F. Braet, Nanotechnology 18 (2007) 412001–412013.
[4] C. Bussy, H. Ali-Boucetta, K. Kostarelos, Acc. Chem. Res. (2012) 692–701.
[5] R.R. Johnson, A. Kohlmeyer, A.T.C. Johnson, M.L. Klein, Nano Lett. 9 (2009) 537–541.
[6] C.C. Chiu, M.C. Maher, G.R. Dieckmann, S.O. Nielsen, ACS Nano 4 (2010) 2539–2546.
[7] K. Balamurugan, V. Subramaniam, Biopolymers 99 (2013) 357–369.
[8] F.T. Arce, H. Jang, S. Ramachandran, P.B. Landon, R. Nussinov, R. Lal, Soft Matter 7 (2011) 5267–5273.
[9] Y. Liu, C. Chipot, X. Shao, W.J. Cai, Phys. Chem. C 115 (2011) 1851–1856.
[10] C.C. Chiu, W. Shinoda, R.H. DeVane, S.O. Nielsen, Soft Matter 8 (2012) 9610–9616.
[11] S.A. Andujar, F. Lugli, S. Höfinger, R.D. Enriz, F. Zerbetto, Phys. Chem. Chem. Phys. 14 (2012) 8599–8607.
[12] M. Mahmoudi, O. Akhavan, M. Ghavami, F. Rezaee, S.M.A. Ghiasi, Nanoscale 4 (2012) 7322–7325.
[13] Z. Fu, Y. Luo, P. Derreumaux, G. Wei, Biophys. J. 97 (2009) 1795–1803.
[14] A.K. Jana, N. Sengupta, Biophys. J. 102 (2012) 1889–1896.
[15] A.K. Jana, J.C. Jose, N. Sengupta, Phys. Chem. Chem. Phys. 15 (2013) 837–844.
[16] J. Hardy, D.J. Selkoe, Science 297 (2002) 353–356.
[17] R. Cappai, K. Barnham, Neurochem. Res. 33 (2008) 526–532.
[18] S. Gnanakaran, R. Nussinov, A.E. Garcia, J. Am. Chem. Soc. 128 (2006) 2158–2159.
[19] S.L. Bernstein, N.F. Dupuis, N.D. Lazo, T. Wyttenbach, M.M. Condron, G. Bitan, D.B. Teplow, J.E. Shea, B.T. Ruotolo, C.V. Robinson, M.T. Bowers, Nat. Chem. 1 (2009) 326–331.
[20] D. Thirumalai, G. Reddy, J.E. Straub, Acc. Chem. Res. 45 (2012) 83–92.
[21] S. Nag, B. Sarkar, A. Bandyopadhyay, B. Sahoo, V.K.A. Sreenivasan, M. Kombrabail, C. Muralidharan, S. Maiti, J. Biol. Chem. 286 (2011) 13827–13833.
[22] J. Khandogin, C.L. Brooks, Proc. Natl. Acad. Sci. 104 (2007) 16880–16885.
[23] N.G. Sgourakis, Y. Yan, S.A. McCallum, C. Wang, A.E. Garcia, J. Mol. Biol. 368 (2007) 1448–1457.
[24] A. Baumketner, J.E. Shea, J. Mol. Biol. 366 (2007) 275–285.
[25] Y. Miller, B. Ma, R. Nussinov, Biophys. J. 97 (2009) 1168–1177.
[26] L. Larini, J.E. Shea, Biophys. J. 103 (2012) 576–586.
[27] S.L. Bernstein, T. Wyttenbach, A. Baumketner, J.E. Shea, G. Bitan, D.B. Teplow, M.T. Bowers, J. Am. Chem. Soc. 127 (2005) 2075–2084.
[28] J. Li, R. Liu, K.S. Lam, L.-W. Jin, Y. Duan, Biophys. J. 100 (2011) 1076–1082.
[29] C. Lockhart, S. Kim, D.K. Klimov, J. Phys. Chem. B 116 (2012) 12922–12932.
[30] W.P. Esler, E.R. Stimson, J.R. Ghilardi, Y.-A. Lu, A.M. Felix, H.V. Vinters, P.W. Mantyh, J.P. Lee, J.E. Maggio, Biochemistry 35 (1996) 13914–13921.
[31] Y.-S. Lin, G.R. Bowman, K.A. Beauchamp, V.S. Pande, Biophys. J. 102 (2012) 315–324.
[32] M.M. Gessel, S. Bernstein, M. Kemper, D.B. Teplow, M.T. Bowers, ACS Chem. Neurosci. 3 (2012) 909–918.
[33] S. Zhang, K. Iwata, M.J. Lachenmann, J.W. Peng, S. Li, E.R. Stimson, Y.-A. Lu, A.M. Felix, J.E. Maggio, J.P. Lee, J. Struct. Biol. 130 (2000) 130–141.
[34] A.T. Petkova, Y. Ishii, J.J. Balbach, O.N. Antzutkin, R.D. Leapman, F. Delaglio, R. Tycko, Proc. Natl. Acad. Sci. U. S. A. 99 (2002) 16742–16747.
[35] J.L. Fauchere, V. Pliska, Eur. J. Med. Chem. 18 (1983) 369–375.
[36] S. Tomaselli, V. Esposito, P. Vangone, N.A.J. van Nuland, A.M.J.J. Bonvin, R. Guerreni, T. Tancredi, P.A. Temussi, D. Picone, ChemBioChem 7 (2006) 257–267.
[37] W. Humphrey, A. Dalke, K. Schulten, J. Mol. Graph. 14 (1996) 33–38.
[38] M. Coles, W. Bicknell, A.A. Watson, D.P. Fairlie, D.J. Craik, Biochemistry 37 (1998) 11064–11077.
[39] O. Crescenzi, S. Tomaselli, R. Guerrini, S. Salvadori, A.M. D'Ursi, P.A. Temussi, D. Picone, Eur. J. Biochem. 269 (2002) 5642–5648.
[40] Y. Xu, J. Shen, X. Luo, W. Zhu, K. Chen, J. Ma, H. Jiang, Proc. Natl. Acad. Sci. U. S. A. 102 (2005) 5403–5407.
[41] C. Lee, S. Ham, J. Comput. Chem. 32 (2010) 349–355.
[42] L. Triguero, R. Singh, R. Prabhakar, J. Phys. Chem. B 112 (2008) 2159–2167.
[43] Q. Wang, J. Zhao, X. Yu, C. Zhao, L. Li, J. Zheng, Langmuir 26 (2010) 12722–12732.

[44] X. Yu, Q. Wang, Y. Lin, J. Zhao, C. Zhao, J. Zheng, Structure, Orientation, and Surface Interaction of Alzheimer Amyloid-β Peptides on the Graphite, Langmuir 28 (2012) 6595–6605.
[45] W.L. Jorgensen, J. Chandrasekhar, J.D. Madura, R.W. Impey, M.L. Klein, J. Chem. Phys. 79 (1983) 926–935.
[46] A.D. MacKerell, D. Bashford, Bellott, R.L. Dunbrack, J.D. Evanseck, M.J. Field, S. Fischer, J. Gao, H. Guo, S. Ha, D. Joseph-McCarthy, L. Kuchnir, K. Kuczera, F.T.K. Lau, C. Mattos, S. Michnick, T. Ngo, D.T. Nguyen, B. Prodhom, W.E. Reiher, B. Roux, M. Schlenkrich, J.C. Smith, R. Stote, J. Straub, M. Watanabe, J. Wiórkiewicz-Kuczera, D. Yin, M. Karplus, J. Phys. Chem. B 102 (1998) 3586–3616.
[47] A.D. Mackerell, M. Feig, C.L. Brooks, J. Comput. Chem. 25 (2004) 1400–1415.
[48] L. Kalé, R. Skeel, M. Bhandarkar, R. Brunner, A. Gursoy, N. Krawetz, J. Phillips, A. Shinozaki, K. Varadarajan, K.J. Schulten, J. Comput. Phys. 151 (1999) 283–312.
[49] J.-P. Ryckaert, G. Ciccotti, H.J.C. Berendsen, J. Comput. Phys. 23 (1977) 327–341.
[50] S.E. Feller, Y. Zhang, R.W. Pastor, B.R. Brooks, J. Chem. Phys. 103 (1995) 4613–4621.
[51] G.J. Martyna, D.J. Tobias, M.L. Klein, J. Chem. Phys. 101 (1994) 4177–4189.
[52] U. Essmann, L. Perera, M.L. Berkowitz, T. Darden, H. Lee, L.G. Pedersen, J. Chem. Phys. 103 (1995) 8577–8593.
[53] E. Darve, D. Rodriguez-Gomez, A. Pohorille, J. Chem. Phys. 128 (2008) 144120–144133.
[54] J. Hénin, G. Fiorin, C. Chipot, M.L. Klein, J. Chem. Theory Comput. 6 (2010) 35–47.
[55] D. Rodriguez-Gomez, E. Darve, J. Chem. Phys. 120 (2004) 3563–3578.
[56] J. Hénin, C. Chipot, J. Chem. Phys. 121 (2004) 2904–2914.
[57] T.E. Creighton, Proteins: Structure and Molecular Properties, 2nd ed., 1993.
[58] S.-H. Chong, S. Ham, Proc. Natl. Acad. Sci. U. S. A. 109 (2012) 7636–7641.
[59] A.P. Minton, Biophys. J. 76 (1999) 176–187.
[60] J.C. Jose, N. Sengupta, Eur. Biophys. J. 42 (2013) 487–494.